The quantum spectrum and the distribution of exceptional points: the hydrogen atom in a strong magnetic field

1994 J. Phys. A: Math. Gen. 27 3059

(http://iopscience.iop.org/0305-4470/27/9/020)

J. Phys. A: Math. Gen. 27 (1994) 3059–3071. Printed in the UK

The quantum spectrum and the distribution of exceptional points: the hydrogen atom in a strong magnetic field

A A Kotzé† and W D Heiss‡

† Department of Applied Mathematics, Rand Afrikaans University, PO Box 524, Aucklandpark 2006, South Africa

‡ Centre for Nonlinear Studies and Department of Physics, University of the Witwatersrand, PO Wits 2050, Johannesburg, South Africa

Received 16 June 1993, in final form 7 January 1994

Abstract. The intricate connection between the distribution of exceptional points and the spectral behaviour of Hamiltonian systems is investigated. A method to determine the distribution of exceptional points for a Hamilton operator with systematic degeneracies is described. Its implementation is demonstrated considering the hydrogen atom in a strong magnetic field. For this case, the distribution of exceptional points is a function of the scaled energy only.

1. Introduction

The subject of 'quantum chaos' has attracted much attention for more than a decade. Yet, a satisfactory definition is still outstanding and general investigations concentrate on the behaviour of systems which have classically chaotic counterparts [1, 2]. In the search for a suitable definition of 'quantum chaos' we investigate the properties of *quantum mechanical (Hamilton) operators* of the form $H_0+\lambda H_1$. The parameter λ plays the role of a perturbation parameter, or it may serve to effect a phase transition or it may even under variation steer the system from an ordered into a chaotic regime [3].

We believe that the exceptional points of a matrix operator will shed light on this fascinating subject [4]. The exceptional points of the full operator are the points λ for which two eigenvalues coalesce. We exclude genuine degeneracies, i.e. the coalescence of two eigenvalues occurs in the complex plane. The physical significance of the exceptional points is due to their relation with the avoided-level crossings for real λ values. Globally, all the exceptional points determine the shape of the real spectrum [5, 6]. A number of authors have studied level dynamics by focusing directly on the spectral properties when the parameter λ is varied. The basic underlying structure of a complicated spectrum has been associated with a soliton [7] in a specific case. Distributions of avoided-level crossings and their gaps have been investigated [8] for matrix models and some real physical systems. Theoretical expressions have been given for random matrix models [9] and deviations from such expressions in real physical systems [10]. In this paper, the focus is directed on the distribution of the exceptional points as they are the underlying mathematical cause for the properties studied by the authors quoted.

The connection between the distribution of the exceptional points and the emergence of quantum chaos is seen as the fundamental mechanism that produces quantum chaos as far as operators of the form $H_0 + \lambda H_1$ are concerned. Here we use the term 'quantum chaos' by referring to the statistical properties of quantum spectra of classically chaotic

0305-4470/94/093059+13$19.50

systems. The positions of the exceptional points are fixed in the complex λ plane and are determined solely by H_0 and H_1. For large matrices, it is, however, prohibitive to determine the positions exactly. Heiss and Kotzé [3] proposed a method to determine the distribution reasonably well from the knowledge of the two operators. Using this method they showed that a high density of exceptional points is a prerequisite for the occurrence of quantum chaos.

Symmetries relating to H_0 and H_1, or both, are usually expected to impose a particular structure on the full problem $H_0 + \lambda H_1$. This also holds when the symmetries relating to the individual operators are incompatible. It is the aim of this paper to study the effect of symmetries on the distribution of the exceptional points and to generalize the method discussed in [3]. From such an analysis we gain further insight into the effect of the exceptional points on the behaviour of a system. As a relevant application, the hydrogen atom in a strong uniform magnetic field is reinvestigated. The major aim of this paper is the demonstration that the exceptional points are relevant and that their distribution can be determined by a relatively inexpensive method. It is for this reason that a well studied problem has been chosen for comparison with quantitative results known from the literature.

2. Exceptional points and the curve spectrum

Avoided-level crossings are always associated with exceptional points [11, 12] if they occur for the levels $E_k(\lambda)$ of the Hamiltonian $H_0 + \lambda H_1$. The exceptional points are square-root branch-point singularities in the complex λ plane and they determine the fluctuation properties of the spectrum [5]. The distribution of exceptional points thus plays a crucial role in the spectral behaviour of the system.

In order to obtain an approximation to the distribution of exceptional points, we utilize the observation that the spectrum of a chaotic system, pertaining to $H_0 + \lambda H_1$, has an underlying simple structure. This structure is imposed on the system through the symmetries of H_0 and H_1 even when the symmetries are incompatible [13, 14]. Below, we describe a procedure to obtain the approximate distribution of exceptional points of a system where H_0 or H_1 (or both) have systematic degeneracies. To this aim we introduce the idea of a *curve spectrum.*

The curve spectrum is obtained by considering Hamiltonians of the form

$$H = D_0 + \lambda U \cdot D_1 \cdot U^{-1} \tag{1}$$

where D_0 and D_1 are the diagonal representations of H_0 and H_1, respectively. The matrix U is an orthogonal matrix and the problem is non-trivial for $U \neq 1$. This particular representation, where H_0 is diagonal, can always be chosen and is suitable for our purpose. We work in an irreducible representation of H to exclude genuine degeneracies for real $\lambda \neq 0$.

2.1. Non-degenerate systems: line spectra

First consider a system without systematic degeneracies and let the eigenvalues of H_0 and H_1 be denoted by ϵ_k and ω_k, respectively. For large values of λ we approximate the eigenvalues $E_k(\lambda)$ of H in equation (1) by a first-order perturbation expansion ($\lambda \gg 1$) i.e. [11]

$$E_k(\lambda) = \alpha_k + \lambda\omega_k + O(1/\lambda). \tag{2}$$

The first two terms of equation (2) yield *lines* with the appropriate association of slopes ω_k and intercepts α_k. Here, α_k are the diagonal elements of the 'backwards' rotated H_0 [3] i.e.

$$\alpha_k = (U^{-1} \cdot H_0 \cdot U)_{k,k}. \tag{3}$$

We term the set of lines in equation (2) the *line spectrum*. They are illustrated as broken lines in figure 1. The line spectrum is an approximation of the actual spectrum.

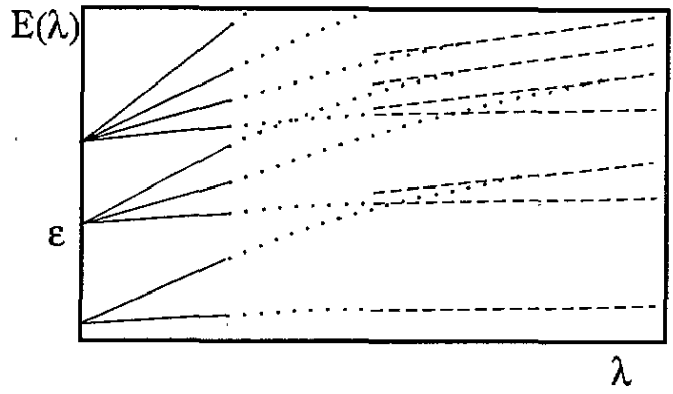

Figure 1. Schematic illustration of the asymptotic curve spectrum for a system that has systematic degeneracies. Here $E_j' = \epsilon_j + \lambda\delta_j$ (full lines), $E_k = \alpha_k + \lambda\omega_k$ (broken lines) *and the dotted curves represent the joining algebraic equations.*

The significance of the line spectrum lies in the fact that the two quantities α_k and ω_k are calculated from knowledge of H_0 and H_1 alone. The line spectrum and the associated $N(N-1)/2$ intersection points are easily calculated. The exceptional points of the full problem are expected to lie near the intersection points of the line spectrum (for the two-dimensional case the real parts of the exceptional points coincide with the points of intersection [11]). From numerical investigations at low dimensions ($N \leqslant 60$), where the actual positions of exceptional points can be determined, we conclude that the distribution of intersection points is statistically equivalent to the distribution of the real parts of the exceptional points [3]. The line spectrum is thus a useful tool for obtaining the statistical properties of the spectrum of the complete system.

2.2. Degenerate systems: curve spectra

If either H_0 or H_1 is degenerate, the number of exceptional points is less than $N(N-1)/2$ depending on the degree of degeneracy. However, the procedure described in the previous section generically yields $N(N-1)/2$ intersection points. This discrepancy affects the distribution of intersection points and hence the anticipated distribution of exceptional points. In the following we describe how the degeneracy of H_0 or H_1 is taken into account.

Suppose that H_0 has systematic degeneracies. We divide the space into p subspaces where each subspace has dimension M_μ; $\mu = 1, 2, \ldots, p$. Each subspace is M_μ-fold degenerate with eigenvalues ϵ_μ. For small values of λ, a first-order perturbation expansion yields eigenvalues of the form $\epsilon_\mu + \lambda\delta_l$ where δ_l are the eigenvalues of H_1 in the μth subspace. This appears as one group of levels originating at ϵ_μ with slopes δ_l in figure 1. The asymptotic ($\lambda \ll 1$) line spectrum for the whole system is therefore

$$E_j' = \epsilon_j + \lambda\delta_j \qquad j = 1, 2, \ldots, M \tag{4}$$

where M is the dimension of the complete system. Note that the line spectrum is again obtainable from quantities easily available from H_0 and H_1 alone.

For an H_0 with degeneracies, equation (2) still holds when $\lambda \gg 1$ and equations (4) and (2) are approximations of the actual spectrum at the respective asymptotic values of λ. The total approximate spectrum is obtained by joining equations (2) and (4) by a simple algebraic equation that only depends on the four quantities ϵ_k, δ_k, α_k and ω_k. The form of this equation is determined by the specific form of the spectrum and is represented by the dotted curves in figure 1. We term this the *curve spectrum* of the system and it signifies the underlying simple structure referred to above. To obtain the curve spectrum, care has to be taken to associate the appropriate E_k in equation (2) with the appropriate E'_k in equation (4). In the following section it is demonstrated how this is achieved in a particular case. For illustration we use as an example the hydrogen atom in a strong magnetic field as it is usually considered as the chaotic system *par excellence* [15–17] and also because of its experimental significance [18].

3. The hydrogen atom in a strong magnetic field

3.1. The model

The Hamiltonian of this system (using atomic units) is

$$H = \frac{p^2}{2} - \frac{1}{r} + \frac{\gamma}{2} l_z + \frac{\gamma^2}{8} r^2 \sin^2\theta. \tag{5}$$

Here γ is a dimensionless parameter giving the field strength and l_z is the z-component of the angular momentum [15]. The azimuthal quantum number m and parity π are good quantum numbers. For the remainder of this paper we will only consider the subspace of positive parity with $m = 0$. The Hamiltonian in equation (5) is now of the form

$$H = H_0 + \lambda H_1 \tag{6}$$

with (scaled by a factor 2)

$$H_0 = p^2 - \frac{2}{r} \qquad H_1 = \frac{1}{4} r^2 \sin^2\theta \qquad \lambda = \gamma^2.$$

Wintgen and Friedrich [19] showed that, similar to the classical system, the behaviour of the quantum system depends only on a scaled energy ε where

$$\lambda = \left(\frac{\varepsilon}{E}\right)^{-3} = [-\varepsilon n^2]^{-3} \tag{7}$$

and where E is the energy and n the principal quantum number [20].

3.2. Matrix representation

In order to discuss the distribution of exceptional points, we use a matrix representation of H with H_0 diagonal, i.e. we use the *Coulomb* basis set [21]. To obtain numerically reliable results, Sturmian functions are used [22]. The subsequent diagonalization of H_0 is done numerically together with the associated rotation of H_1.

Wunner *et al* [23] proposed the following orthonormal and complete set of Sturmian functions as the radial eigenfunctions

$$G_{nl}^{(\zeta)}(r) = \zeta^{3/2}\sqrt{\frac{(n-l-1)!}{(n+l+1)!}}\mathrm{e}^{-\zeta r/2}[\zeta r]^l L_{n-l-1}^{2l+2}(\zeta r) \tag{8}$$

with L_{n-l-1}^{2l+2} denoting the generalized Laguerre polynomials, ζ is a positive real parameter and $n = 1, 2, \ldots, n_{\max}$ is the principal quantum number where $n_{\max}$ is the maximum n considered in the truncated matrix space. Using equation (8) (and Schrödinger's radial integrals [25]) yields a matrix representation for H in (6) [4,26] which is the most efficient approach close to the ionization threshold [17]. The explicit formulae are listed in appendix A.

The advantage of this basis lies in the freedom of choice for the parameter ζ, which serves to control convergence and accuracy. We choose $\zeta = 2/n^*$ ($n^* = 1, 2, 3, \ldots, n$) for accurate eigenvalues in the vicinity of n^* [24]. Valuable computing time is thus saved when extremely accurate eigenvalues have to be computed. The range of accurate eigenvalues can be extended by choosing $n_{\max}$ to be considerably larger than n^*, but, with a corresponding increase in computing time and memory usage.

For calculating the eigenvalues, curve spectrum and determining the density of exceptional points the following scheme is appropriate for (n, l)

$$(1,0), (2,0), (3,0), (3,2), (4,0), (4,2), (5,0), (5,2), (5,4), \ldots, (n_{\max}, n_{\max}-1). \tag{9}$$

This order leads to a full matrix H_0 while H_1 has a block structure. The order used for (n, l) in equation (9) is a reshuffling of the order generally used in the literature. This has been appropriately taken into account when truncating the matrices. We have tested our procedure against the procedures described in the literature by comparing the eigenvalues so obtained with those by Friedrich and Wintgen [15], Delande and Gay [27], Killingbeck [28] and Clark and Taylor [24]. The eigenvalues were found to be accurate under due variation of the parameter ζ.

A part of the spectrum is drawn in figure 2 for $n = 34, 35, \ldots, 42$ with energy measured in Rydbergs. Here $n_{\max} = 50$ and $\zeta = 2/40$ resulting in a 650×650 matrix which can easily be evaluated and diagonalized on a minisuper computer. The strength parameter λ is taken between 0 and 10^{-9} which corresponds to a field strength of between 0 and 7.43 Tesla. At $\lambda = 0$ the degeneracies of the pure hydrogen atom are genuine; for $\lambda > 0$ the lines do not cross but undergo avoided-level crossings.

3.3. Curve spectrum for hydrogen

By scanning the spectrum in figure 2, the underlying simple structure becomes obvious if all the avoided-level crossings are taken as real crossings. We recall that at $\lambda = 0$ the crossings are actual degeneracies of H_0; all other crossings are level repulsions which look like actual crossings due to the resolution used. The simple and structured form of the spectrum is expected since the symmetries relating to H_0 and H_1 impose a particular structure on the full problem $H_0 + \lambda H_1$. In other words, while the detailed structure of the spectrum looks rather complex, *an underlying simple structure is discernible.* This simple structure is simulated through the curve spectrum obtained explicitly below.

Having transformed to a representation with H_0 diagonal we use the guidelines given in section 2.2. Each principal quantum number n is degenerate in the angular momentum

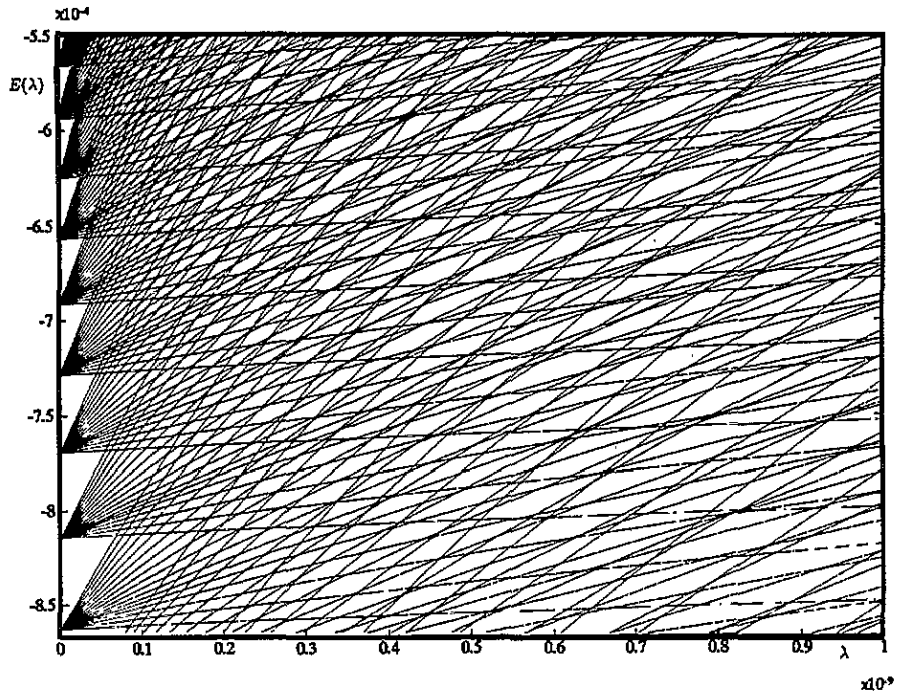

Figure 2. The spectrum for the hydrogen atom in a uniform magnetic field. The part shown is with strength parameter λ between 0 and 10^{-9}, the principal quantum number $n = 34, 35, \ldots, 42$ (from bottom to top) and the energy is measured in Rydbergs.

quantum number l. The subspaces are characterised by n and we denote them as n-subspaces. To obtain explicitly the curve spectrum, we find the appropriate connection of E_k and E'_k (equations (2) and (4), respectively) by noting the following. First, the individual lines in each n-subspace do not intersect one another. Second, the order of the lines for increasing values of λ is given by the fact that the top-most line of the n-subspace crosses all the lines of the $(n+1)$-subspace except the top-most one; the second top line crosses all the lines of the $(n+1)$-subspace except the second top and top-most lines etc, the first line of the n-subspace does not cross any lines of the $(n+1)$-subspace.

A simple curve which connects E_k and E'_k is given by the heuristic algebraic equation

$$\tilde{E}_k(\lambda) = \alpha_k + \lambda\delta_k - [|\alpha_k - \epsilon_k|^{3/2} + \lambda^{3/2}|\delta_k - \omega_k|^{3/2}]^{2/3}. \tag{10}$$

The value of the power 2/3 is found to fit sufficiently well. The form of equation (10) ensures that it reduces to equations (2) and (4) when $\lambda \to \infty$ and $\lambda \to 0$ respectively. By construction, the curve spectrum coincides with the spectrum of the truncated matrix $H_0 + \lambda H_1$ only asymptotically for $\lambda \ll 1$ and $\lambda \gg 1$. In particular, for $\lambda \gg 1$ it shares all deficiencies of a spectrum obtained numerically by truncation. In the region of interest, which is the middle region, the curve spectrum does not reproduce the details of the spectrum obtained by diagonalization for each value of λ. However, it does reproduce the distribution of the real parts of the exceptional points to the point of quantitative agreement with known results as demonstrated below. We recall that this result is obtained from quantities that can be derived from H_0 and H_1 alone.

In order for equation (10) to give the appropriate curve spectrum all the lines should have negative curvature. This can only hold if the following inequalities

$$\alpha_k > \epsilon_k \qquad \delta_k > \omega_k \tag{11}$$

are obeyed. Because α_k and ϵ_k are obtained by rotations of the same matrix D_0, they obey the same trace rules and (11) cannot hold globally. However, we found that (11) is always satisfied in the vicinity of n^* as long as $n_{max} \geqslant 2n^*$, i.e. for the middle range of the spectrum. Figure 3 shows the line spectrum for the same window of the actual spectrum drawn in figure 2. The similarity between the actual and curve spectrum is striking. Here $n_{max} = 90$ and $n^* = 40$ which leads to a matrix of order 2070×2070 to be diagonalized. This procedure is very efficient because the diagonalization has to be done only once to obtain the four quantities α, ϵ, ω and δ for a specific n^*.

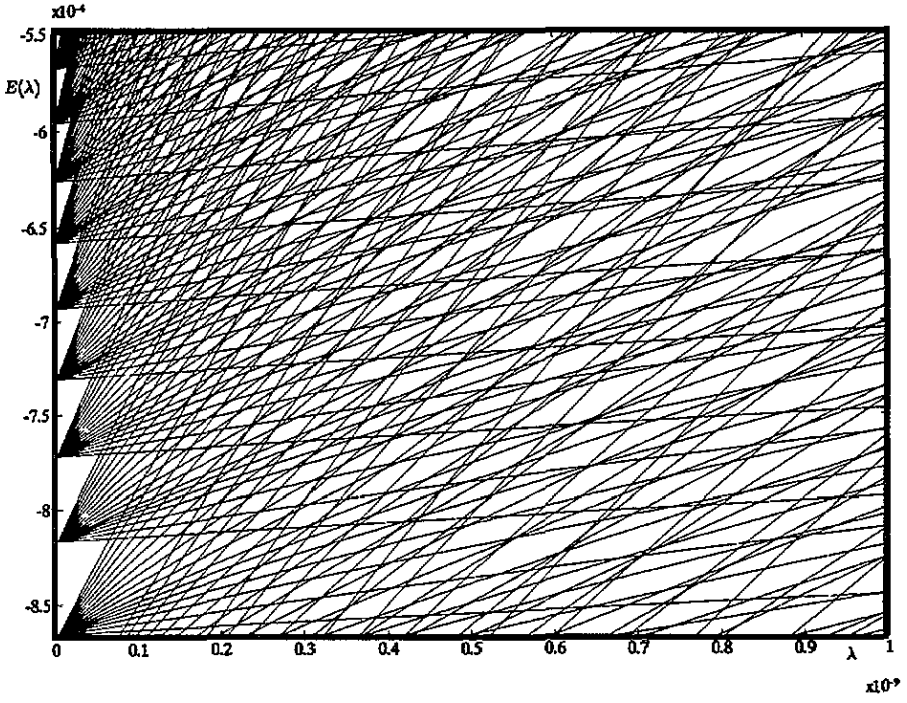

Figure 3. Curve spectrum for the hydrogen atom in a magnetic field. For the sake of comparison the same E and λ values as those depicted in figure 2 are shown.

The curve spectrum is now used to obtain the density of exceptional points from the intersection points. All calculations are done for constant scaled energy ε. The actual intersections of the curves are easily calculated using a standard Newton–Raphson numerical procedure.

3.4. Density of exceptional points

A suitable representation of the distribution of intersection points is obtained by keeping n^* fixed. The distribution is then calculated by choosing a 'window' between two scaled energies ε_1 and ε_2 where the top and bottom energies are defined by setting $n^*_{1,2} = n^* \pm 2$.

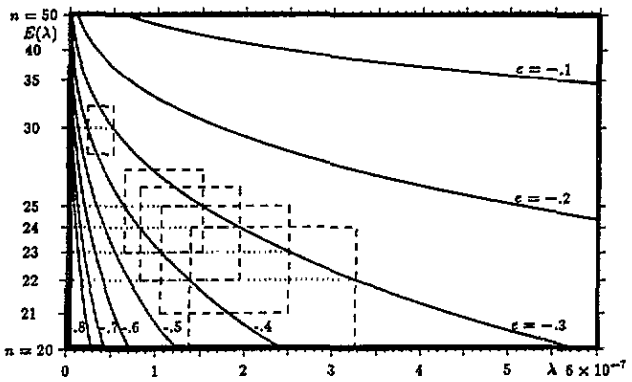

Figure 4. Schematic representation of the 'windows' (broken rectangles) used to calculate the distribution of intersection points. The full curves are the invariant lines with values of the scaled energy ε indicated.

The left and right λ's are obtained by setting $\lambda_1 = [-\varepsilon_1(n^*)^2]^{-3}$ and $\lambda_2 = [-\varepsilon_2(n^*)^2]^{-3}$. Here we have $\lambda_1 < \lambda_2$ and $\varepsilon_2 < \varepsilon_1$. This is schematically shown as one 'window' (broken rectangle) in figure 4.

The distribution of intersection points P in a 'window' of length $\varepsilon_2 - \varepsilon_1$ is then calculated. The area under the histogram, so obtained, is normalized to unity so that P can be related for different n^*-values, thus allowing different 'windows' to be compared. To render a direct comparison between the quantal and classical results, we took many overlapping 'windows' ($n^* = 15, 16, 17, \ldots, 45$) and calculated the distribution in each (see figure 4). The total distribution of intersections $P = P(n^*, \varepsilon_2 - \varepsilon_1)$ is represented in a contour graph in figure 5 with $\varepsilon_1 = -0.5$ and $\varepsilon_2 = -0.2$. The lines shown are constant P lines, each with a different value for P. The global decreasing nature of P with increasing scaled energy is evident.

From figure 5 we make two observations: first, for fixed n^*, the normalized density of intersections P decreases with increasing ε and second, statistically, the normalized density of exceptional points does not depend on n^* (and thus the energy E) or λ *but only on the scaled energy* ε.

The first observation confirms the fact, which is evident from the spectrum in figure 2, that the density of states decreases if n^* is fixed and ε increased. This is expected since there is a relation between the density of states and the density of intersections given by P. The distribution P does not relate to the fact that the density of states increases if ε is kept fixed, and n^* is increased, because of the normalization procedure used. The actual density of intersections, i.e. the absolute count of the number of intersections without normalization $P'(n^*)$ for ε fixed, is plotted in figure 6 for $\varepsilon = -0.2$. This clearly shows that the larger the value of n^* is, the higher the density of intersection points. Since we deal with a particular situation and are unaware of a quantitative relationship between P' and n^*, we use a least-square fit and find

$$P'_\varepsilon(n^*) = an^* + b(n^*)^2 + c(n^*)^3. \tag{12}$$

Note that the leading term is cubic in n^*. As can be seen from table 1, equation (12) holds for all relevant values of ε.

Of great significance is the second observation which is consistent with results from a classical and quantum mechanical analysis in that the only relevant parameter is the scaled

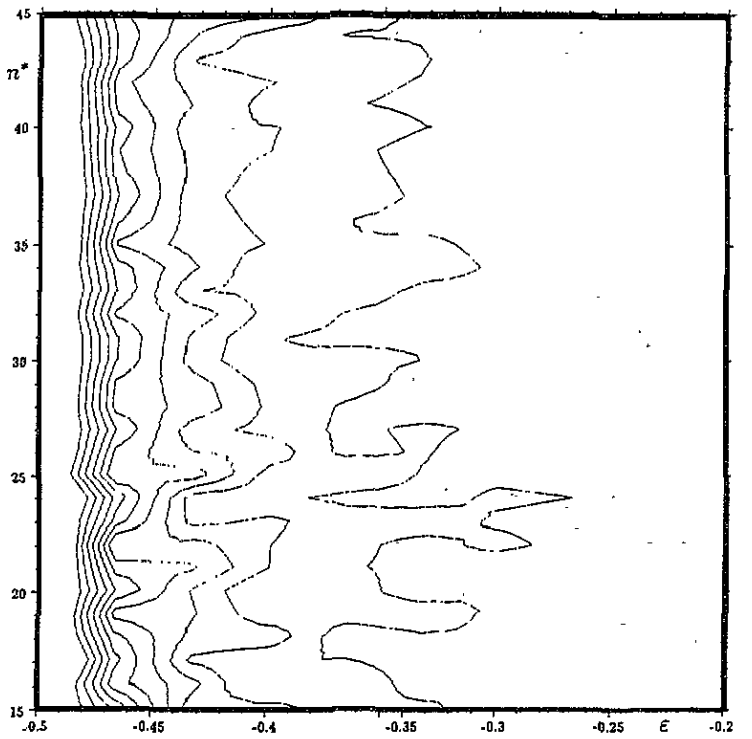

Figure 5. A geographical map (contour graph) showing that the density of intersection points only depends on the scaled energy ε. The full lines are lines of constant density of crossing points P with the higher values on the left side of the graph. The declining nature of P which is constant in principal quantum number n^* is evident.

Table 1. Least-square fits to the actual density of intersections $P'_\varepsilon(n^*)$ for several values of the scaled energy ε.

$P'_{-0.2} = -0.66387n^* + 0.04843(n^*)^2 + 0.0016(n^*)^3$
$P'_{-0.3} = 1.62276n^* - 0.08895(n^*)^2 + 0.00232(n^*)^3$
$P'_{-0.4} = -0.58714n^* + 0.03823(n^*)^2 + 0.00065(n^*)^3$
$P'_{-0.5} = -0.50964n^* + 0.02749(n^*)^2 + 0.00089(n^*)^3$
$P'_{-0.6} = 0.08612n^* - 0.01368(n^*)^2 + 0.00137(n^*)^3$
$P'_{-0.8} = 0.89097n^* - 0.04718(n^*)^2 + 0.00502(n^*)^3$

energy ε [15]. It holds, in particular, for the normalized density of intersection points. This is a non-trivial result in the context of the present paper. While a corresponding observation has been made by other authors [8, 10], we obtained it from the density of the exceptional points and not by diagonalizing $H_0 + \lambda H_1$ for a large range of λ-values. The curve spectrum is an auxiliary device to determine from the intersection points the geometrical distribution of the real parts of the exceptional points. The result obtained confirms the fact that the mathematical mechanism which determines the properties of the spectrum of the Hamiltonian $H_0 + \lambda H_1$ must be sought in the exceptional points. On a technical point, we stress that the result has been obtained without determining explicitly the positions of the exceptional points which is in fact prohibitive in view of their huge number (about half a million for the matrix size considered).

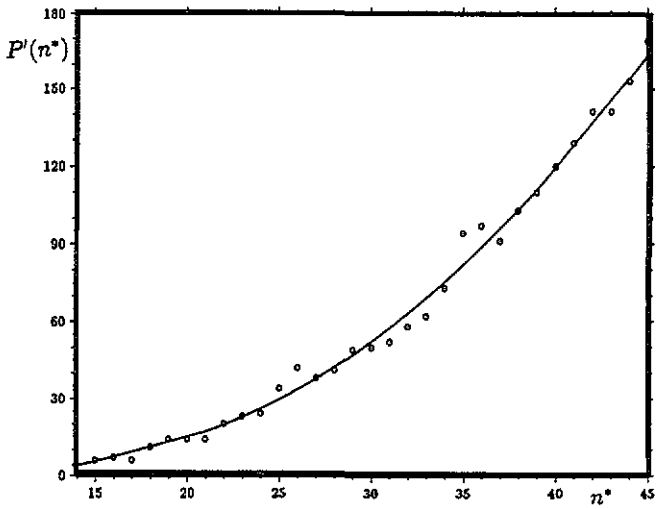

Figure 6. Actual density of crossings P' as a function of principal quantum number n^* shown for scaled energy $\varepsilon = -0.2$. The full curve is a least-square fit given by P'_ε (see table 1).

4. The role of the imaginary parts of the exceptional points

From the findings above we conclude that the density of exceptional points is higher for $\varepsilon_1 = -0.5$ than for $\varepsilon_2 = -0.2$. Yet we know that the system behaves more chaotically for larger ε. Chaos sets in at $\varepsilon \approx -0.35$ and the system is fully chaotic for $\varepsilon = -0.1$ [20]. This is only an apparent contradiction to the conjecture [3], that a higher density of exceptional points makes chaos more likely to occur. In fact, if the bulk of the exceptional points is situated close to the real axis, the corresponding level repulsions are only weakly pronounced which yields a Poisson rather than a Wigner distribution for the nearest-neighbour spacing distribution [11]. In physical terms, this situation corresponds to very weak mixing which is due to small coupling matrix elements. It is known that it is the density of states and the coupling matrix elements [29] that influence the fluctuations of the spectrum; if the mean distance of the levels is of the same order of magnitude as the coupling matrix elements, conditions are most favourable for fluctuations associated with quantum chaos. The density of intersections of the unperturbed curves is related to the density of states while the coupling matrix elements determine, in particular, the imaginary part of the exceptional points which in turn determine the fluctuation properties of the spectrum. This latter information is not contained in the intersection points since it is the coupling which moves the exceptional points into the complex plane. Roughly speaking, the quotient of the imaginary and real part of the exceptional point is proportional to the coupling matrix element. The energy gap between repelling levels is also proportional to the same quantities.

The leading term of $P'_\varepsilon(n^*)$ is cubic in n^*. It turns out that the average growth of the coupling matrix is also proportional to $[n^*]^3$. When moving on a line of constant scaled energy ε, the coupling parameter λ decreases proportionally to $(n^*)^{-6}$. Hence the product $P'_\varepsilon(n^*) \times \lambda \times H_1^{\text{average}}$ is essentially constant when moving on an invariant line. We have here the interesting situation that the increasing density of levels (exceptional points) is balanced by the corresponding inverse behaviour of λH_1.

5. Summary and discussion

The hydrogen atom in a strong uniform magnetic field has been re-examined by investigating the distribution of exceptional points. The curve spectrum which exhibits the underlying simple structure of the actual spectrum can be obtained from the two operators H_0 and H_1 alone. The distribution of intersection points of the curve spectrum reflects the distribution of the real parts of the exceptional points. Regions of high density of these distributions are a prerequisite to the exhibition of chaotic behaviour. If the coupling between the levels is sufficiently strong, the onset of chaotic behaviour is expected precisely in that region.

The study of hydrogen in a strong magnetic field is used as a test case for the universally valid fact that all properties of the spectrum of an operator of the form $H_0 + \lambda H_1$ must reside in the exceptional points. While this is obvious from a mathematical point of view, we have demonstrated that it can be used in practical terms in a non-trivial situation. We have established that the results of our analysis are in line with known results in that the relevant distributions depend only on the scaled energy ε.

At this point one might speculate about further developments. The symmetries of either H_0 or H_1 (or both) impose structure onto the spectrum. In the spectrum of the hydrogen atom in a magnetic field there are, in addition, scaling laws. The latter structure has been re-established in this paper. The former structure is expected to relate the distribution of exceptional points to the classical periodic orbits. Work on simple matrix models reveals that such a relation exists [13, 14]. It is hoped that with further progress along these lines we will be able to explain the semiclassical results by the detailed structure of the positions of the exceptional points.

Appendix A. Matrix representations of H_0 and H_1

Using the Sturmian function basis given in (8) and the radial integral due to Schrödinger [25] leads to a matrix representation of H_0 given by

$$\langle 0, l', n'|H_0|n, l, 0\rangle = -\frac{\zeta^2}{4}\delta_{n',n}\delta_{l',l} + \zeta^2\sqrt{\frac{(n-l-1)!}{(n+l+1)!}}\sqrt{\frac{(n'-l'-1)!}{(n'+l'+1)!}}\sum_{\tau=0}^{\leqslant \frac{n-l-1}{n'-l'-1}}\frac{(2l+\tau)!}{\tau!}$$
$$\times[(n-l-1)(n-l-\tau)(n'-l-\tau) + (n-2/\zeta)(2l+\tau+1)$$
$$-(n+l+1)(n-l-1-\tau)(n'-l-\tau)]\delta_{l',l}.$$

Here $\sum_{\tau=0}^{\leqslant \frac{n-l-1}{n'-l'-1}}$ means that τ runs to the smaller of the two numbers. The matrix representation of H_0 is diagonal in l but not in n. Using (8), the matrix elements for H_1 can also be expressed in closed analytical form. The matrix is banded according to the selection rules $|n-n'| \leqslant 2$ and $|l-l'| = 0, 2$. Using Schrödinger's radial integral, the radial matrix elements $H_r = \langle l', n'|r^2|n, l\rangle$ are found [4]. When $l' = l$

$$n' = n-2 : H_r = \zeta^{-2}\sqrt{(n-l-2)(n-l-1)(n+l)(n+l+1)}$$

$$n' = n-1 : H_r = -4n\zeta^{-2}\sqrt{(n-l-1)(n+l+1)}$$

$$n' = n : H_r = 2\zeta^{-2}[3n(n+1) - l(l+2)]$$

$$n' = n+1 : H_r = -4(n+1)\zeta^{-2}\sqrt{(n-l)(n+l+2)}$$

$$n' = n+2 : H_r = \zeta^{-2}\sqrt{(n-l+1)(n-l)(n+l+2)(n+l+3)}$$

and for $l' = l + 2$

$$n' = n - 2 : H_r = \zeta^{-2}\sqrt{(n-l-1)(n-l-2)(n-l-3)(n-l-4)}$$

$$n' = n - 1 : H_r = -4\zeta^{-2}\sqrt{(n-l-1)(n-l-2)(n-l-3)(n+l+2)}$$

$$n' = n : H_r = 6\zeta^{-2}\sqrt{(n-l-1)(n-l-2)(n+l+2)(n+l+3)}$$

$$n' = n + 1 : H_r = -4\zeta^{-2}\sqrt{(n-l-1)(n+l+2)(n+l+3)(n+l+4)}$$

$$n' = n + 2 : H_r = \zeta^{-2}\sqrt{(n+l+2)(n+l+3)(n+l+4)(n+l+5)}$$

and for $l' = l - 2$

$$n' = n - 2 : H_r = \zeta^{-2}\sqrt{(n+l-2)(n+l-1)(n+l)(n+l+1)}$$

$$n' = n - 1 : H_r = -4\zeta^{-2}\sqrt{(n+l-1)(n+l)(n+l+1)(n-l)}$$

$$n' = n : H_r = 6\zeta^{-2}\sqrt{(n+l)(n+l+1)(n-l)(n-l+1)}$$

$$n' = n + 1 : H_r = -4\zeta^{-2}\sqrt{(n+l+1)(n-l)(n-l+1)(n-l+2)}$$

$$n' = n + 2 : H_r = \zeta^{-2}\sqrt{(n-l)(n-l+1)(n-l+2)(n-l+3)}.$$

Acknowledgment

AAK wishes to express his gratitude to K T Taylor for introducing him to the Sturmian basis set used by Wunner *et al* [23].

References

[1] Gutzwiller M C 1990 *Chaos in Classical and Quantum Mechanics* (Berlin: Springer)
[2] Ozorio de Almeida A M 1988 *Hamiltonian Systems: Chaos and Quantisation* (Cambridge: Cambridge University Press)
[3] Heiss W D and Kotzé A A 1991 *Phys. Rev.* A 44 2403
[4] Kotzé A A 1992 *PhD Thesis* University of the Witwatersrand, Johannesburg
[5] Heiss W D and Sannino A L 1991 *Phys. Rev.* A 43 4159
[6] Heiss W D and Steeb W-H 1991 *J. Math. Phys.* 32 3003
[7] Gaspard P, Rice S A and Nakamura K 1989 *Phys. Rev. Lett.* 63 930
[8] Zakrzewski J and Kuś M 1991 *Phys. Rev. Lett.* 67 2749
Zakrzewski J, Delande D and Kuś M 1993 *Phys. Rev.* E 47 1665
[9] Wilkinson M 1989 *J. Phys. A: Math. Gen.* 22 2795
[10] Goldberg J and Schweizer W 1991 *J. Phys. A: Math. Gen.* 24 2785
[11] Heiss W D and Sannino A L 1990 *J. Phys. A: Math. Gen.* 23 1167
[12] Shanley P E 1989 *Ann. Phys., NY* 186 292
[13] Heiss W D and Chiang J C H 1993 *Phys. Rev.* A 47 2533
[14] Heiss W D and Müller M 1993 *Phys. Rev.* A 48 2558
[15] Friedrich H and Wintgen D 1989 *Phys. Rep.* 183 37
[16] Garstang R H 1977 *Rep. Prog. Phys.* 40 105
[17] Taylor K T 1990 *Atoms in Strong Fields (NATO ASI Series B)* vol 212, ed C A Nicolaides *et al* (New York: Plenum)

[18] Main J, Wiebusch G, Holle A and Welge K H 1986 *Phys. Rev. Lett.* **57** 2789
Koch P E 1992 *Chaos and Quantum Chaos (Lecture Notes in Physics 411)* (Berlin: Springer)
[19] Wintgen D and Friedrich H 1987 *Phys. Rev.* A **36** 131
[20] Wintgen D and Friedrich H 1987 *Phys. Rev.* A **35** 1464
[21] Zimmerman M L 1987 *Phys. Rev.* A **35** 1464
Kash M M and Kleppner D 1980 *Phys. Rev. Lett.* **45** 1092
[22] Rotenberg M 1970 *Adv. At. Mol. Phys.* **6** 233
[23] Wunner G, Kost M and Ruder H 1986 *Phys. Rev.* A **33** 1444
[24] Clark C W and Taylor K T 1982 *J. Phys. B: At. Mol. Phys.* **15** 1175
[25] Schrödinger E 1926 *Ann. Phys.* **80** 483
[26] Zeller G 1990 *PhD Thesis* University of Tübingen
[27] Delande D and Gay J C 1986 *J. Phys. B: At. Mol. Phys.* **19** L173
[28] Killingbeck J 1979 *J. Phys. B: At. Mol. Phys.* **12** 25
[29] Guhr T and Weidenmüller H A 1990 *Ann. Phys., NY* **199** 412